AGU ADVANCING EARTH AND SPACE SCIENCE

Geophysical Research Letters

RESEARCH LETTER
10.1029/2021GL094421

Key Points:

- Orbital eccentricity variations on 100 Myr timescales drive changes in ice shell thickness
- Downward-propagating cracks can reach the subsurface ocean on Enceladus but do not reach Europa's ocean
- On Enceladus, eruptions are likely sustained by decompression boiling

Supporting Information:

Supporting Information may be found in the online version of this article.

Correspondence to:

M. L. Rudolph,
maxrudolph@ucdavis.edu

Citation:

Rudolph, M. L., Manga, M., Walker, M., & Rhoden, A. R. (2022). Cooling crusts create concomitant cryovolcanic cracks. *Geophysical Research Letters*, *49*, e2021GL094421. https://doi.org/10.1029/2021GL094421

Received 20 MAY 2021
Accepted 9 FEB 2022

Cooling Crusts Create Concomitant Cryovolcanic Cracks

Maxwell L. Rudolph[1], Michael Manga[2], Matthew Walker[3], and Alyssa R. Rhoden[4]

[1]Department of Earth and Planetary Sciences, University of California, Davis, CA, USA, [2]Department of Earth and Planetary Science, University of California, Berkeley, CA, USA, [3]Planetary Science Institute, Tucson, AZ, USA, [4]Southwest Research Institute, Boulder, CO, USA

Abstract The orbital and internal evolution of the ice-covered ocean worlds orbiting Jupiter and Saturn are coupled, leading to time-varying thicknesses of their ice shells. As the ice thickens and thins, thermal stresses in the ice shell and pressure in the underlying ocean will change, promoting and hindering fracturing of the ice shell. We identify when and at what depth cracks initiate and whether they can penetrate the entire ice shell. For an ice tensile strength of 3 MPa, cracks do not penetrate the ice shell of Europa. On Enceladus, time-averaged ice shell thickness of less than 15 km and variations in tidal dissipation of more than 15% over approximately 100 Myr eccentricity cycles cause cracks to cross the ice shell and permit eruptions from the ocean. Ocean overpressure is never large enough to extrude water onto the surface, suggesting that eruptions on Enceladus are sustained by decompression boiling.

Plain Language Summary Saturn's moon Enceladus has an ongoing eruption fed by a subsurface ocean. Jupiter's moon Europa may have active or recent eruptions as well. The processes that allow these eruptions to occur are not entirely understood. Changes in the orbits of Europa and Enceladus on 100 Myr timescales lead to time-varying tidal dissipation, driving changes in ice shell thickness. One mechanism for creating cracks (which could evolve into cryovolcanic conduits) is related to thickening of an ice shell. The volume change associated with the solidification of water to ice produces global tensile stresses in the ice shell and increases the pressure in the ocean. We model this process and conclude that it is a viable mechanism to explain the formation of cracks that reach the ocean on Enceladus. However, owing to larger gravitational acceleration, we do not expect cracks to reach the subsurface ocean on Europa.

1. Introduction

Cryovolcanism is actively occurring on Saturn's moon Enceladus (Porco et al., 2006), may be occurring on Europa over multidecadal timescales (Jia et al., 2018; Paganini et al., 2020; Roth, Retherford, et al., 2014), and may occur on other icy bodies (e.g., Geissler, 2015). The eruption of mixtures of ice, gas, and water requires the existence of a pathway through which material can ascend. Eruptions can be driven by a combination of buoyancy of the cryovolcanic mixture, overpressure in the subsurface ocean or reservoir (Fagents, 2003; Manga & Wang, 2007), by the exsolution and expansion of dissolved gases (e.g., Crawford & Stevenson, 1988), or by decompression boiling (Ingersoll & Nakajima, 2016; Nakajima & Ingersoll, 2016). When a planetary ice shell thickens or thins due to solidification or melting at the ocean-ice interface, two phenomena occur simultaneously that can drive cryovolcanism. First, the volume change as liquid water solidifies increases pressure within the subsurface ocean. In turn, this pushes the ice shell outwards, generating global tensile stresses. Second, as the ice shell thickness evolves, the changing temperature gradient generates thermal stresses within the ice shell. Both of these processes can generate 10^0 MPa stresses (Manga & Wang, 2007; Nimmo, 2004)—an order of magnitude larger than stresses associated with tidal deformations—and large enough to overcome the tensile strength of intact water ice.

Europa and Enceladus have orbits that interact with other satellites of Jupiter and Saturn, respectively, providing a mechanism to drive secular change in orbital parameters and, hence, tidal dissipation. Europa participates in a 4:2:1 mean motion resonance (MMR) with Ganymede and Io. Europa's orbital eccentricity may vary on timescales of 10^2–10^3 Myr (Hussmann & Spohn, 2004). Enceladus is presently in a 2:1 MMR with Dione. For some combinations of Saturn's tidal quality factor Q and Enceladus' internal structure, Enceladus' orbital eccentricity and internal heating may vary on timescales of 10^2 Myr (Shoji et al., 2014).

The volume increase associated with solidification at the ocean-ice interface will lead to uplift (radial displacement) of a thickening planetary ice shell. This produces tensile stresses, which are countered by thermal contraction associated with a decreasing geothermal gradient (Nimmo, 2004). The volume change associated with solidification also causes the overpressure in a subsurface ocean to increase. In the absence of thermal stresses, and assuming a tensile strength of 1–3 MPa (Dempsey et al., 1999; Ultee et al., 2020), the global tensile stresses associated with ocean pressurization can overcome the tensile strength of ice after 10^2–10^3 m of thickening on both Enceladus and Europa (Manga & Wang, 2007). Again ignoring the near-surface compression associated with thermal stresses, it is conceivable for cracks that initiate at the surface, where tensile stresses are largest, to propagate downward and reach a subsurface ocean. In order to do so, cracks must be able to penetrate the viscous sublayer of an ice shell, where the deviatoric elastic stresses associated with ice shell thickening relax. Based on calculations that did not include the thermal contraction effect, Rudolph and Manga (2009) showed that cracks could reach a subsurface ocean on Enceladus but that the stronger gravity on Europa could prevent downward-propagating cracks from reaching the subsurface ocean.

We revisit the problem of stresses generated within ice shells subjected to thickening and thinning due to time-varying tidal dissipation. We develop a coupled model that describes ice shell thermal evolution, the stresses within the ice shell due to ocean overpressure and thermoelasticity, and the response of the ice shell to crack formation. We model the depth to which cracks penetrate and determine the conditions under which cracks reach the subsurface ocean. We apply this model to cyclic changes in ice shell thickness driven by periodically varying tidal dissipation.

2. Methods

The planetary ice shell is idealized as a spherical shell with homogeneous and isotropic elastic properties and temperature-dependent viscosity. The use of geometrically and physically simplified models enables a characterization of the first-order controls on the dynamics of a complex system and permits a complete exploration of parameter space (e.g., Turcotte & Schubert, 2002). Nevertheless, we acknowledge that in taking this approach, some processes and properties are not incorporated. For instance, lateral variations in ice shell thickness and physical properties can significantly affect the amount and distribution of tidal heating (Beuthe, 2013; Čadek et al., 2019; Pleiner Sládková et al., 2021; Souček et al., 2019).

Here, we present the equations governing the conduction of heat in the ice shell, the stresses $\left(\underline{\underline{\sigma}}\right)$, and the mechanical coupling between ocean pressurization and thermal evolution. At each timestep, we apply the following procedure: (a) calculate the amount of solidification/melting at the ocean-ice interface, (b) solve for temperature, (c) solve for the principal stress acting in the radial direction (σ_r), (d) calculate the principal stress in the tangential direction (σ_t), strains, and displacements. We iterate (c, d) as needed to obtain stresses and displacements that are compatible with the overpressure in the ocean.

2.1. Thermal Model

The temperature distribution in the ice shell is governed by the diffusion equation, expressed here in spherical coordinates

$$\rho_i C_p \frac{\partial T}{\partial t} = \frac{1}{r^2}\frac{\partial}{\partial r}\left(r^2 k \frac{\partial T}{\partial r}\right) + H, \tag{1}$$

where r denotes the radial coordinate, T is temperature, ρ_i is ice density, C_p is heat capacity, H is the volumetric rate of internal heating, and t is time. We apply an isothermal boundary condition $T(r_o) = 100$ K at the surface (r_o). The thermal conductivity k of ice is temperature-dependent, varying by a factor of approximately 3 from 100 K to the melting temperature (e.g., Carnahan et al., 2021). We use $k(T) = 651/T$ for T in Kelvin and k in W m^{-1} K^{-1} (Petrenko & Whitworth, 1999). Because the internal heating produced by tidal dissipation is concentrated in the warm ice near the base of a conductive ice shell (e.g., Nimmo & Manga, 2009), we approximate H with a basal heat flux q_b that includes heat produced within the ice shell and heat transported from the deeper interior.

We discretize Equation 1 using conservative finite differences in space and an implicit scheme in time. At the beginning of each timestep, we estimate the amount of ice that solidifies at the ocean-ice interface (Δz) by balancing the heat conducted upwards with the energy released by solidification

$$\Delta z = -\frac{k\Delta t}{\rho_i L} \left.\frac{\partial T}{\partial r}\right|_{r=r_i(t)}, \tag{2}$$

where L is the latent heat of fusion, Δt is the time step, and r_i denotes the inner radius of the ice shell. We move the bottom of the domain and use linear interpolation to transfer the temperature and stress fields from the previous timestep onto the new grid (Nimmo, 2004). We limit the timestep so that the ocean-ice interface never moves more than half of the grid spacing.

2.2. Mechanical Model

We solve the equations governing the thermo-visco-elastic deformation in a spherical shell. A complete derivation of the governing equations, which closely follows Hillier and Squyres (1991) and Nimmo (2004), is given in Text S2 in Supporting Information S1. The mechanical structure of the ice shell is determined primarily by the strong temperature-dependence of viscosity. The viscosity is given by

$$\mu(T) = \mu_b \exp\left(\frac{Q\,(T_b - T)}{RT_bT}\right) \tag{3}$$

where μ_b is the melting-point (T_b) viscosity, Q is an activation energy, and R is the universal gas constant (Nimmo, 2004). We use an activation energy $Q = 40$ kJ/mol, leading to viscosity variations of 13 orders of magnitude between T_b and 100 K. We neglect mushy layers that might develop during thickening (Buffo et al., 2021). Additional material properties are given in Table S1 in Supporting Information S1. We carried out tests with the nonlinear composite rheology of Goldsby and Kohlstedt (1997) and Goldsby and Kohlstedt (2001) and did not observe significant differences from models that used only a temperature-dependent viscosity (Text S5, Figures S2-S4 in Supporting Information S1).

We assume a tensile strength of 3 MPa, a value consistent with the largest values obtained from experiments on intact specimens of first year sea ice (Dempsey et al., 1999). The repeated failure of ice may reduce the strength of ice, particularly within the cold near-surface ice, where damage anneals slowly (Hammond et al., 2018). An additional set of models was computed with a lower tensile strength of 1 MPa, summarized in Figure S1 in Supporting Information S1. These 10^0 MPa estimates of tensile strength are an order of magnitude larger than the diurnal tidal stresses of 100 kPa on Europa (Greenberg et al., 1998; Hurford, Sarid, & Greenberg, 2007) or Enceladus (Hurford, Helfenstein, et al., 2007), suggesting that additional stress sources (such as ocean pressurization) are necessary to crack an intact ice shell.

2.3. Ocean Pressurization

The excess pressure in the ocean is calculated using equation 5 from Manga and Wang (2007),

$$P_{ex} = \frac{3r_i^3}{\beta\left(r_i^3 - r_c^3\right)}\left[\frac{z\,(\rho_w - \rho_i)}{\rho_w} - u_r\right] \tag{4}$$

where u_r is the (outward) radial displacement at the base of the ice shell, β is the compressibility of the ocean, r_c is the radius of the rocky core, z is the amount of ice shell thickening, and ρ_i and ρ_w are the densities of ice and water, respectively.

2.4. Failure and Yielding

We consider the failure and yielding of the ice shell in the tensile and compressive regimes. When the tensile stress exceeds the tensile strength of ice, a crack forms. We assume that once a crack forms, it propagates on

timescales shorter than the viscous relaxation timescale and reaches a maximum depth at which depth-integrated tensile loading is balanced by depth-integrated lithostatic compression. This force-balance condition was found to accurately describe the depth of penetration of isolated cracks (Hemingway et al., 2020; Rudolph & Manga, 2009). These crack propagation calculations used a boundary element method based on linear elastic fracture mechanics that accounts for the crack-tip stresses and the stress concentration effects associated with the free surface and the deformable boundary at the ocean-ice interface (Hemingway et al., 2020; Rudolph & Manga, 2009). The interaction of multiple adjacent cracks, not considered here, would reduce the maximum depth of penetration (Walker et al., 2021).

When failure occurs, we follow a multistep process to assign the maximum (z_b) and minimum (z_t) depths reached by the crack. Starting from the depth at which tensile stresses first exceed tensile strength z_0, we calculate the net tensile loading (including the contribution from lithostatic stress) acting on the crack above the depth of initial failure as $F_{\text{net}}(z_t) = \int_{z_0}^{z_t} \sigma_t(z) dz$. We assume that the crack will propagate upward until $F_{\text{net}}(z_t) = 0$. If F_{net} remains positive even for z_t extending to the surface, we assume that the crack reaches the surface and find z_b that satisfies $\int_{z_b}^{z_t} \sigma_t(z) dz = 0$. If the crack is arrested below the surface, we assume that the crack extends downwards to z_b that satisfies $\int_{z_b}^{z_0} \sigma_t(z) dz = 0$. In our models, all cracks able to reach the subsurface ocean also reached the surface.

We assume that a crack relieves tensile stresses at depths between z_t and z_b. Stress relief is implemented by reducing the Maxwell time of the material in the cracked region to 1/10 of the timestep and taking 10 small (1 year) timesteps in order to relieve deviatoric elastic stresses. We performed resolution tests and observed no differences in the evolution of stresses and ocean overpressure or the timing of cracking events associated with taking 1 versus 10 small timesteps or reducing the Maxwell time to 1/10 or 1/100 of the timestep.

2.5. Eruptions

In the absence of additional sources of buoyancy (such as volatile expansion and exsolution), water will rise only to the level at which ocean pressure balances the weight of the water column. The critical excess pressure needed to extrude water onto the surface is $P_{\text{ex,crit}} = (\rho_w - \rho_i)(r_o - r_i)g$ (Manga & Wang, 2007). The level to which water rises due to overpressure would be reduced in the presence of porous ice or dissolved salts in the ocean (Lee et al., 2005; Nimmo et al., 2003). However, even if water does not reach the surface, decompression boiling can sustain eruptions of vapor and water (Ingersoll & Nakajima, 2016; Nakajima & Ingersoll, 2016).

3. Results

We calculate the stresses in an ice shell subjected to time-varying basal heat flux q_b of the form $q_b = q_0 + \Delta q \sin(\omega t)$ where q_0 is average heat flux and ω is the angular frequency of perturbation. We consider equilibrium ice shell thickness values of 2–30 km. For both Europa and Enceladus, we consider oscillations with a period of 100 Myr based on the models of coupled thermal and orbital evolution of the Jovian and Saturnian systems in Hussmann and Spohn (2004) and Shoji et al. (2014). We vary the time-averaged ice shell thickness (related to the average heat flow q_0) and the amplitude of heat flux perturbations, parameterized as $\Delta q/q_0$. The tensile stresses, timing, and depth of cracking events, and existence of ocean-reaching cracks are shown for two specific scenarios in Figure 1.

During each 100 Myr eccentricity cycle, cracks initiate below the surface during the thickening phase. In successive cracking events, failure begins at increasing depth as the thickness of the elastic ice increases. Figure 2 summarizes the number and depth extent of cracking events per 100 Myr cycle. The fractional penetration (depth of penetration divided by ice shell thickness) of cracks increases with decreasing equilibrium thickness and with increasing $\Delta q/q_0$. The frequency of cracking events generally increases with decreasing equilibrium thickness and with increasing $\Delta q/q_0$.

On Europa, we predict that cracks will penetrate at most approximately 48% of the ice shell. Because cracks do not reach the ocean, eruptions are not predicted.

Cracks reach the ocean on Enceladus for time-averaged ice shell thicknesses <15 km and heat flux perturbation amplitudes $\Delta q/q_0 \geq 0.15$. The ocean overpressure at the time of eruption is not sufficient to extrude water onto

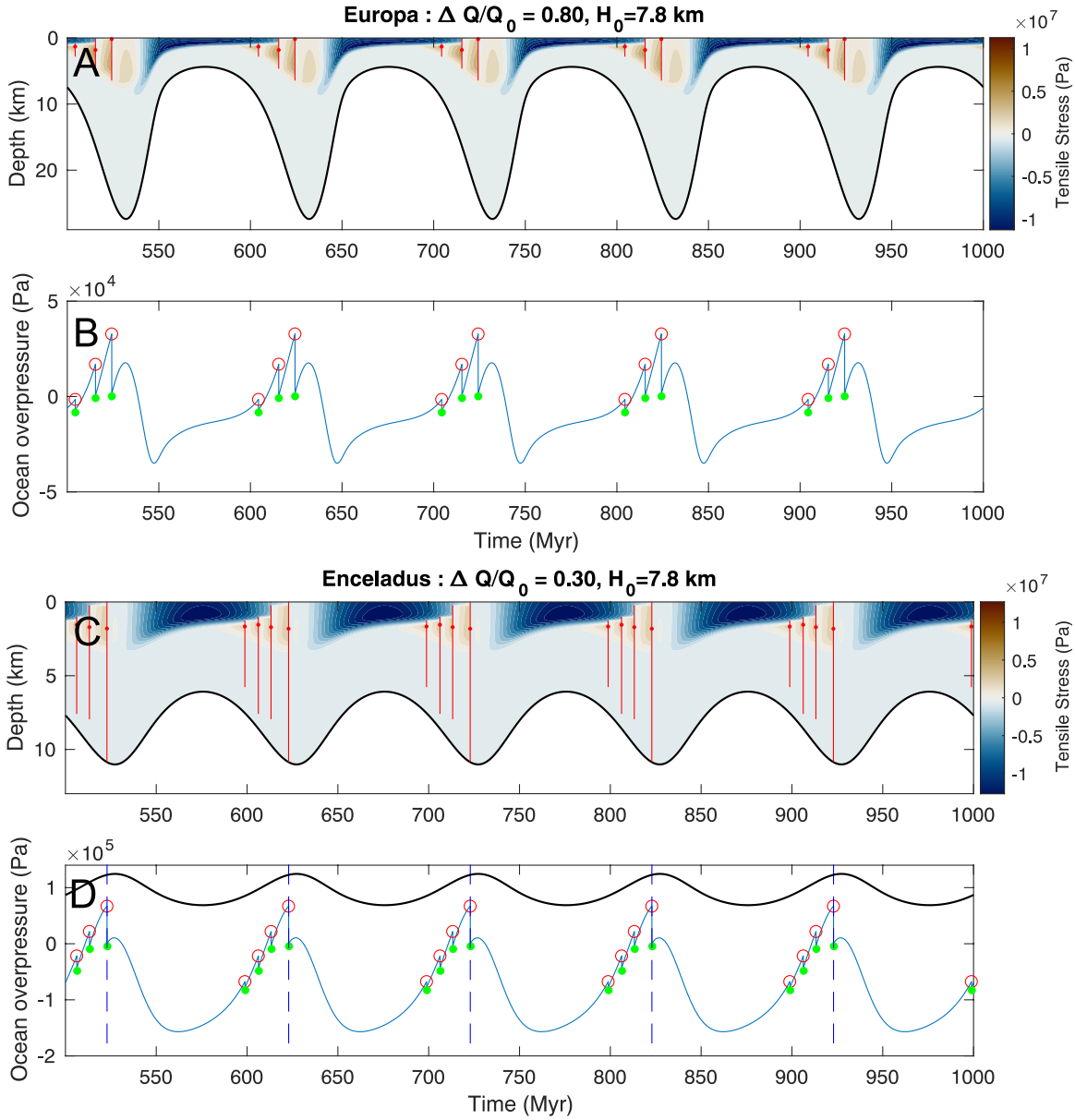

Figure 1. Evolution of ice shell thickness and tangential stress σ_t under Europa-like (a) and Enceladus-like (c) conditions. Red vertical lines indicate the occurrence and depth-exent of tensile cracks, and red points indicate the depth of initial failure. Panels (b) and (d) show the evolution of ocean overpressure. The black curve in (d) indicates the critical overpressure necessary to extrude water onto the surface. Red and green circles indicate the overpressure before and after cracks form. The blue-dashed vertical lines (d) indicate the formation of cracks that spans the entire ice shell. On Enceladus, some, but not all, cracks reach the subsurface ocean. On Europa, no cracks reach the ocean.

the surface without additional sources of buoyancy. However, we expect that decompression boiling (Ingersoll & Nakajima, 2016; Nakajima & Ingersoll, 2016) and tidal dissipation within cracks can permit sustained eruptions (Kite & Rubin, 2016). On average, the first eruption follows a minimum in ice shell thickness by 25 Myr. The standard deviation of this lag among all of the ice shell thickness and $\Delta q/q_0$ values shown Figures 2 and 3 is 3.3 Myr.

The tensile strength of ice limits the maximum tensile stress that can occur in the ice shell. Thus, for lower values of the tensile strength, cracks do not penetrate as deeply. For a tensile strength of 1 MPa, cracks reach Enceladus' ocean only for time-averaged ice shell thicknesses less than 4.5 km (Figure S1 in Supporting Information S1).

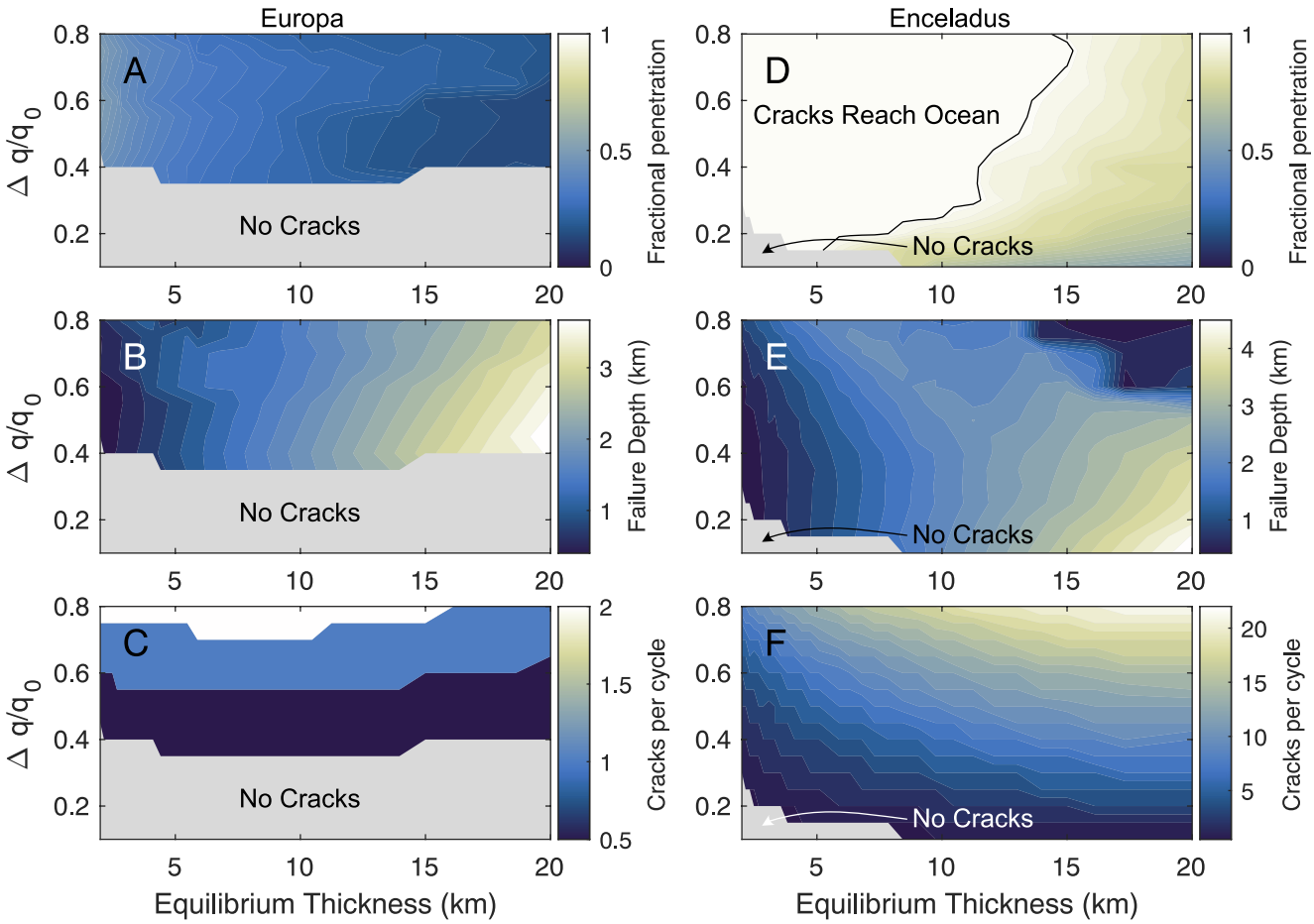

Figure 2. Dynamics of cracks on Europa (left) and Enceladus (right). (a, d) The depth of crack penetration, expressed as a fraction of ice shell thickness. The black contour in (d) encloses the conditions under which cracks reach the subsurface ocean. The median depth at which tensile stresses exceed the tensile strength is shown in (b, e). (c, f) Number of crack formation events per 100 Myr eccentricity cycle.

4. Discussion

We calculated the thermal and mechanical response of a planetary ice shell subjected to periodic, sinusoidal variations in basal heat flux. We do not expect downward-propagating cracks to reach a subsurface ocean on Europa (Figure 2a). On Enceladus, the weaker gravitational acceleration enables downward-propagating cracks to reach the ocean (Figure 2b). In general, increasing the amplitude of heat flow variations leads to larger changes in ice shell thickness and therefore larger stresses and more failure events per 100 Myr eccentricity cycle.

The dissociation products of water vapor have been detected near Europa using Hubble Space Telescope emission line spectroscopy (Roth, Saur, et al., 2014) and by analyzing absorption features as Europa occults Jupiter (Sparks et al., 2016, 2017). Water vapor has been observed spectroscopically on 1 of 17 observations using the 10 m Keck Telescope (Paganini et al., 2020). There is geologic evidence for the eruption of liquid water, including the presence of smooth, low-albedo deposits that fill topographic lows and raised lenticular features that may have formed as viscous extrusions at the surface (Fagents, 2003; Lesage et al., 2021; Miyamoto et al., 2005; Quick et al., 2017). Salts and non-ice material appear to be concentrated near chaos and along lineaments (McCord et al., 1999). Some mechanical models for the formation of Europa's double ridges (Greenberg et al., 1998), triple bands (Fagents et al., 2000), blocky chaos (Schmidt et al., 2011), and lenticular features (Miyamoto et al., 2005; Michaut & Manga, 2014; Quick et al., 2017; Singer et al., 2021) invoke the presence of liquid water at or near the surface.

We did not identify any cases in which downward-propagating cracks reach a subsurface ocean on Europa. While this is a negative result, it does not preclude the formation of cryovolcanic conduits via other processes. Upward

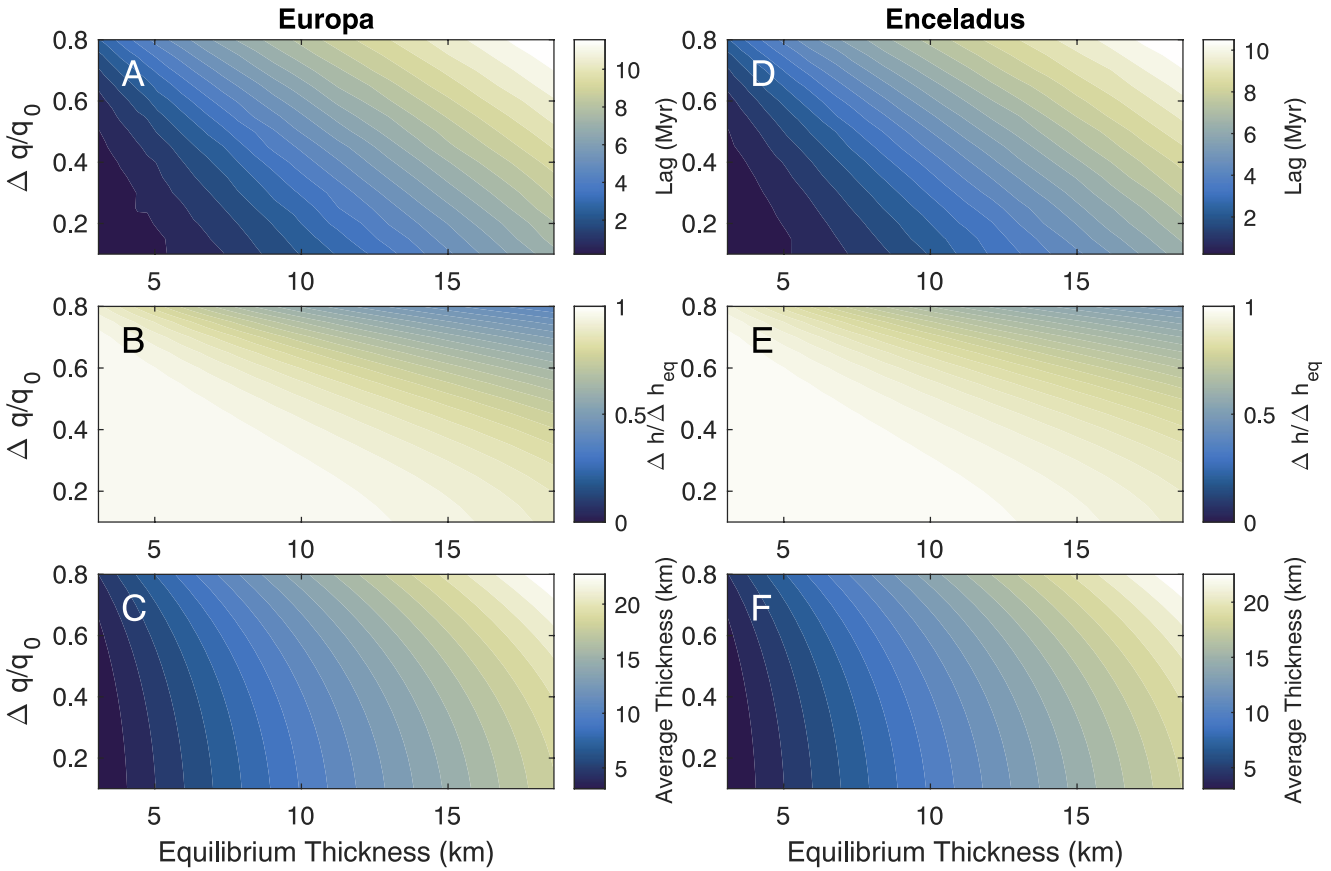

Figure 3. Departure from steady-state behavior. (a, d) Time delay (lag) between the minimum dissipation and the maximum ice shell thickness. In panels (b, e) we show the ratio of the range of thicknesses observed (Δh) to the range of thicknesses that would be attained under equilibrium conditions (Δh_{eq}). Panels (c) and (f) show the actual average ice shell thickness. The period of the oscillations in dissipation is 100 Myr in all cases.

propagation of cracks is mechanically challenging due to the relaxation of stresses in the warm ice near the ocean-ice interface. The growth of upward-propagating cracks might occur by stress-corrosion cracking (Porco et al., 2014), but laboratory experiments do not find a reduction in strength after cyclic deformation (Hammond et al., 2018). Exsolved volatiles could provide a source of stresses (associated with buoyancy) that drives upward propagation of cracks (Crawford & Stevenson, 1988). Melt may be generated in situ by localized tidal heating, particularly if the salt content of Europa's ice shell is variable (O'Brien et al., 2002; Sotin et al., 2002; Vilella et al., 2020) or by frictional heating along faults (Nimmo & Gaidos, 2002). If water is present within Europa's icy crust, water pockets may become pressurized and generate upward-propagating cracks that reach the surface (Fagents, 2003; Lesage et al., 2020; Neveu et al., 2015; Wilson et al., 1997). Finally, impacts may directly or indirectly lead to the eruption of water (Steinbrügge et al., 2020).

Our results demonstrate that for a broad range of equilibrium ice shell thicknesses and heat flux perturbations, downward-propagating tensile cracks may reach a subsurface ocean on Enceladus. Cracks penetrate more deeply on Enceladus because gravity is an order of magnitude weaker than on Europa. The tiger stripe fissures on Enceladus are clear examples of shell-breaching pathways that enable eruptions of ocean water as plumes (Postberg et al., 2009). In addition to the tiger stripes, Enceladus' south polar terrain contains intersecting double-ridged cracks that predate the tiger stripes (Patthoff & Kattenhorn, 2011). These cracks are straighter, narrower, and shorter than the tiger stripe fissures (though they may be truncated by more recently formed faults). The background of older cracks in the south polar terrain suggests a geologically recent change in Enceladus' activity, perhaps linked to the onset of a cooling episode that led to the formation of newer cracks.

Hemingway et al. (2020) proposed that the tiger stripes at Enceladus' south pole formed via a cascading failure mechanism in which the first crack is generated by the ocean overpressure mechanism and subsequent cracks

form due to bending stresses. Our models demonstrate the feasibility of producing an initial crack for ice shell thicknesses up to 15 km, compatible with estimates of Enceladus' present-day ice shell thickness of 20 km on average and 5–14 km near the south pole (Hemingway & Mittal, 2019). Although the models employed here assume spherical symmetry and uniform ice shell thickness, we expect that cracks would form preferentially where ice is thinner, concentrating stresses. Prior to the formation of the tiger stripes, we expect that the polar regions were thinnest due to spatial variations in tidal dissipation (Tobie et al., 2008) and instabilities in ice shell dynamics (Kang & Flierl, 2020). The cascading failure mechanism does not appeal to impact processes (e.g., Roberts & Stickle, 2021; Siraj & Loeb, 2021).

Our models predict that ice shell thickness variations can be significantly out of phase with variations in tidal dissipation, even for the 100 Myr forcing considered here. The lag between minima in dissipation and maxima in ice shell thickness increases with increasing equilibrium thickness and with increasing amplitude of dissipation variations (Figures 3a and 3d). The largest lags are approximately 10 Myr for the parameters considered here. The adjustment of ice shell thickness to increasing versus decreasing dissipation is asymmetric. When dissipation increases, the thinning response of the ice shell is rapid because dissipation occurs near the ocean-ice interface and the rate of thinning is linearly proportional to the power dissipated. On the other hand, when dissipation decreases, the rate of thickening is limited by the upward conduction of heat, which is inversely proportional to ice shell thickness. Because a thinner ice shell adjusts more quickly to changes in heat flow, the ice shell is closer to equilibrium during positive excursions in dissipation. Thus, the observed thickness variations are smaller in amplitude than what would be predicted from the variations in dissipation (Figures 3b and 3e). The asymmetry in response to changes in dissipation leads to time-averaged ice shell thickness that can be significantly thicker than the equilibrium thickness for a given value of q_0 (Figures 3c and 3f).

The ability of cracks to reach the subsurface ocean depends on the assumed tensile strength of ice, which limits the maximum tensile stresses that can exist in the ice shell. Constraints on the mechanical properties of ice are offered by laboratory experiments and by modeling the behavior of glaciers, ice sheets, sea ice, and planetary ice shell processes. The largest tensile strength measured for intact, fine-grained laboratory specimens is 1.5 MPa at −10°C (Schulson, 2001). Polycrystalline ice with smaller grain size exhibits larger tensile strength. Terrestrial sea ice is weaker than laboratory specimens and its strength is strongly scale-dependent, with tensile strength values decreasing from approximately 0.5 to 0.05 MPa for 0.1–2 m scales (Dempsey et al., 1999). For terrestrial sea ice at temperatures greater than the NaCl-H_2O eutectic (−35°C), variations in brine volume fraction lead to decreasing tensile strength with increasing temperature (Schulson, 2001; Weeks, 1962). The tensile strength inferred from modeling some glacial processes (approximately MPa) is comparable to that of laboratory specimens and 10–100 times larger than that of sea ice (e.g., Ultee et al., 2020). The tensile strength of a planetary ice shell after many failure events over several cycles is likely to be lower than the upper limit indicated by laboratory specimens.

Tensile cracks are observed on Europa's surface parallel to some double-ridges, and the formation of these cracks in response to surface loads can be used, in principle, to estimate the in-situ tensile strength of ice. Billings and Kattenhorn (2005) used the spacing between ridge-parallel cracks and the central trough of double ridges to constrain the elastic thickness of Europa's ice shell under the assumption of a line load on a broken elastic plate (Turcotte & Schubert, 2002). Assuming a line load of approximately 6×10^7 kg/m (estimated from the dimensions of Androgeos Linea), we estimate maximum bending stresses at the surface of 10^{-1} MPa, noting that this estimate is highly uncertain due to the uncertainties in the Young's modulus and elastic thickness. These flanking cracks do not appear to accumulate tectonic offsets and do not appear to be linked to cryovolcanic processes, suggesting that they may be superficial cracks that only penetrate highly fractured, weakened ice near the surface.

Convection may be occurring within the ice shells of Europa (e.g., Pappalardo et al., 1998) and Enceladus (e.g., Barr & McKinnon, 2007), but the style of convection and the relationship between surface features and convective upwellings and are not entirely understood (Howell & Pappalardo, 2018). In a convecting ice shell, the fractional thickness of the elastic layer is smaller than for a purely conductive shell, owing to the steeper temperature gradient near the surface. This would make downward-propagating cracks less likely to reach an ocean. Changes in the pattern of convection in a thickening ice shell would lead to a more complex thickening history (Allu Peddinti & McNamara, 2019). Due to more efficient upward heat transport, a convecting ice shell can also adjust more rapidly to decreases in tidal heating (Green et al., 2021).

5. Conclusions

We modeled the evolution of stresses in the ice shells of Europa and Enceladus due to changes in ice shell thickness driven by 100 Myr variations in orbital eccentricity. Changes in ice shell thickness generate thermal stresses due to the changing thermal gradient and global tensile stresses due to the volume change as water freezes to ice. Downward-propagating tensile cracks reach the subsurface ocean on Enceladus for plausible combinations of ice shell thickness and variations in tidal dissipation. On Europa, the generation of downward-propagating tensile cracks is inhibited and cracks do not reach the subsurface ocean. The presence of multiple, interacting, cracks further reduces the depth to which cracks can penetrate (Walker et al., 2021). Our models involve key mathematical simplifications, including the assumption of uniform ice shell thickness and tidal heating. In future work, it would be useful to consider the joint influence of thermal and ocean pressurization stresses, which can reach several MPa, and the 0.1 MPa tidal stresses to interpret the timing and location of crack formation and the development of tidally controlled cracks.

Data Availability Statement

The computer code necessary to reproduce all numerical results and figures is available on Zenodo (doi: 10.5281/zenodo.5551865).

Acknowledgments
The authors thank the editor, Andrew Dombard, and three anonymous reviewers. Michael Manga, Alyssa R. Rhoden, and Matthew Walker thank NASA for financial support.

References

Allu Peddinti, D., & McNamara, A. K. (2019). Dynamical investigation of a thickening ice-shell: Implications for the icy moon Europa. *Icarus*, *329*, 251–269. https://doi.org/10.1016/j.icarus.2019.03.037

Barr, A. C., & McKinnon, W. B. (2007). Convection in Enceladus' ice shell: Conditions for initiation. *Geophysical Research Letters*, *34*(9), 09202. https://doi.org/10.1029/2006GL028799

Beuthe, M. (2013). Spatial patterns of tidal heating. *Icarus*, *223*(1), 308–329. https://doi.org/10.1016/j.icarus.2012.11.020

Billings, S. E., & Kattenhorn, S. A. (2005). The great thickness debate: Ice shell thickness models for Europa and comparisons with estimates based on flexure at ridges. *Icarus*, *177*, 397–412. https://doi.org/10.1016/j.icarus.2005.03.013

Buffo, J. J., Schmidt, B. E., Huber, C., & Meyer, C. R. (2021). Characterizing the ice-ocean interface of icy worlds: A theoretical approach. *Icarus*, *360*, 114318. https://doi.org/10.1016/j.icarus.2021.114318

Čadek, O., Souček, O., Běhounková, M., Choblet, G., Tobie, G., & Hron, J. (2019). Long-term stability of Enceladus' uneven ice shell. *Icarus*, *319*, 476–484. https://doi.org/10.1016/j.icarus.2018.10.003

Carnahan, E., Wolfenbarger, N. S., Jordan, J. S., & Hesse, M. A. (2021). New insights into temperature-dependent ice properties and their effect on ice shell convection for icy ocean worlds. *Earth and Planetary Science Letters*, *563*, 116886. https://doi.org/10.1016/j.epsl.2021.116886

Crawford, G. D., & Stevenson, D. J. (1988). Gas-driven water volcanism in the resurfacing of Europa. *Icarus*, *73*(1), 66–79. https://doi.org/10.1016/0019-1035(88)90085-1

Dempsey, J. P., Adamson, R. M., & Mulmule, S. V. (1999). Scale effects on the in-situ tensile strength and fracture of ice. Part II: First-year sea ice at Resolute, N.W.T. *International Journal of Fracture*, *95*(1), 347–366. https://doi.org/10.1007/978-94-011-4659-3_19

Fagents, S. A. (2003). Considerations for effusive cryovolcanism on Europa: The post-Galileo perspective. *Journal of Geophysical Research*, *108*(E12), 5139. https://doi.org/10.1029/2003JE002128

Fagents, S. A., Greeley, R., Sullivan, R. J., Pappalardo, R. T., Prockter, L. M., & Team, T. G. S. (2000). Cryomagmatic mechanisms for the formation of Rhadamanthys Linea, triple band Margins, and other low-albedo features on Europa. *Icarus*, *144*(1), 54–88. https://doi.org/10.1006/icar.1999.6254

Geissler, P. (2015). Chapter 44 - cryovolcanism in the outer solar system. In H. Sigurdsson (Ed.), *The encyclopedia of volcanoes* (2nd ed., pp. 763–776). Academic Press. https://doi.org/10.1016/b978-0-12-385938-9.00044-4

Goldsby, D. L., & Kohlstedt, D. L. (1997). Grain boundary sliding in fine-grained ice I. *Scripta Materialia*, *37*(9), 1399–1406. https://doi.org/10.1016/s1359-6462(97)00246-7

Goldsby, D. L., & Kohlstedt, D. L. (2001). Superplastic deformation of ice: Experimental observations. *Journal of Geophysical Research*, *106*(B6), 11017–11030. https://doi.org/10.1029/2000JB900336

Green, A. P., Montesi, L. G. J., & Cooper, C. M. (2021). The growth of Europa's icy shell: Convection and crystallization. *Journal of Geophysical Research: Planets*, *126*(4), e2020JE006677. https://doi.org/10.1029/2020JE006677

Greenberg, R., Geissler, P., Hoppa, G., Tufts, B. R., Durda, D. D., Pappalardo, R., et al. (1998). Tectonic processes on Europa: Tidal stresses, mechanical response, and visible features. *Icarus*, *135*(1), 64–78. https://doi.org/10.1006/icar.1998.5986

Hammond, N. P., Barr, A. C., Cooper, R. F., Caswell, T. E., & Hirth, G. (2018). Experimental constraints on the fatigue of icy satellite lithospheres by tidal forces. *Journal of Geophysical Research: Planets*, *123*(2), 390–404. https://doi.org/10.1002/2017je005464

Hemingway, D. J., & Mittal, T. (2019). Enceladus's ice shell structure as a window on internal heat production. *Icarus*, *332*, 111–131. https://doi.org/10.1016/j.icarus.2019.03.011

Hemingway, D. J., Rudolph, M. L., & Manga, M. (2020). Cascading parallel fractures on Enceladus. *Nature Astronomy*, *4*(3), 234–239. https://doi.org/10.1038/s41550-019-0958-x

Hillier, J., & Squyres, S. W. (1991). Thermal stress tectonics on the satellites of Saturn and Uranus. *Journal of Geophysical Research (ISSN)*, *96*, 15665–15674. https://doi.org/10.1029/91JE01401

Howell, S. M., & Pappalardo, R. T. (2018). Band formation and ocean-surface interaction on Europa and Ganymede. *Geophysical Research Letters*, *45*(10), 4701–4709. https://doi.org/10.1029/2018gl077594

Hurford, T. A., Helfenstein, P., Hoppa, G. V., Greenberg, R., & Bills, B. G. (2007). Eruptions arising from tidally controlled periodic openings of rifts on Enceladus. *Nature*, *447*, 292–294. https://doi.org/10.1038/nature05821

Hurford, T. A., Sarid, A. R., & Greenberg, R. (2007). Cycloidal cracks on Europa: Improved modeling and non-synchronous rotation implications. *Icarus*, *186*, 218–233. https://doi.org/10.1016/j.icarus.2006.08.026

Hussmann, H., & Spohn, T. (2004). Thermal-orbital evolution of Io and Europa. *Icarus*, *171*(2), 391–410. https://doi.org/10.1016/j.icarus.2004.05.020

Ingersoll, A. P., & Nakajima, M. (2016). Controlled boiling on Enceladus. 2. Model of the liquid-filled cracks. *Icarus*, *272*, 319–326. https://doi.org/10.1016/j.icarus.2015.12.040

Jia, X., Kivelson, M. G., Khurana, K. K., & Kurth, W. S. (2018). Evidence of a plume on Europa from Galileo magnetic and plasma wave signatures. *Nature Astronomy*, *2*(6), 459–464. https://doi.org/10.1038/s41550-018-0450-z

Kang, W., & Flierl, G. (2020). Spontaneous formation of geysers at only one pole on Enceladus's ice shell. *Proceedings of the National Academy of Sciences*, *117*(26), 14764–14768. https://doi.org/10.1073/pnas.2001648117

Kite, E. S., & Rubin, A. M. (2016). Sustained eruptions on Enceladus explained by turbulent dissipation in tiger stripes. *Proceedings of the National Academy of Sciences*, *113*(15), 3972–3975. https://doi.org/10.1073/pnas.1520507113

Lee, S., Pappalardo, R. T., & Makris, N. C. (2005). Mechanics of tidally driven fractures in Europa's ice shell. *Icarus*, *177*, 367–379. https://doi.org/10.1016/j.icarus.2005.07.003

Lesage, E., Massol, H., & Schmidt, F. (2020). Cryomagma ascent on Europa. *Icarus*, *335*, 113369. https://doi.org/10.1016/j.icarus.2019.07.003

Lesage, E., Schmidt, F., Andrieu, F., & Massol, H. (2021). Constraints on effusive cryovolcanic eruptions on Europa using topography obtained from Galileo images. *Icarus*, *361*, 114373. https://doi.org/10.1016/j.icarus.2021.114373

Manga, M., & Wang, C.-Y. (2007). Pressurized oceans and the eruption of liquid water on Europa and Enceladus. *Geophysical Research Letters*, *34*, L07202. https://doi.org/10.1029/2007GL029297

McCord, T. B., Hansen, G. B., Matson, D. L., Jonhson, T. V., Crowley, J. K., Fanale, F. P., et al. (1999). Hydrated salt minerals on Europa's surface from the Galileo near-infrared mapping spectrometer (NIMS) investigation. *Journal of Geophysical Research*, *104*, 11827–11851. https://doi.org/10.1029/1999JE900005

Michaut, C., & Manga, M. (2014). Domes, pits, and small chaos on Europa produced by water sills. *Journal of Geophysical Research*, *119*(3), 550–573. https://doi.org/10.1002/2013je004558

Miyamoto, H., Mitri, G., Showman, A. P., & Dohm, J. M. (2005). Putative ice flows on Europa: Geometric patterns and relation to topography collectively constrain material properties and effusion rates. *Icarus*, *177*, 413–424. https://doi.org/10.1016/j.icarus.2005.03.014

Nakajima, M., & Ingersoll, A. P. (2016). Controlled boiling on Enceladus. 1. Model of the vapor-driven jets. *Icarus*, *272*, 309–318. https://doi.org/10.1016/j.icarus.2016.02.027

Neveu, M., Desch, S. J., Shock, E. L., & Glein, C. R. (2015). Prerequisites for explosive cryovolcanism on dwarf planet-class Kuiper belt objects. *Icarus*, *246*, 48–64. https://doi.org/10.1016/j.icarus.2014.03.043

Nimmo, F. (2004). Stresses generated in cooling viscoelastic ice shells: Application to Europa. *Journal of Geophysical Research*, *109*, E12001. https://doi.org/10.1029/2004JE002347

Nimmo, F., & Gaidos, E. (2002). Strike-slip motion and double ridge formation on Europa. *Journal of Geophysical Research*, *107*(E4), 5021. https://doi.org/10.1029/2000JE001476

Nimmo, F., & Manga, M. (2009). Geodynamics of Europa's icy shell. In *Europa* (pp. 381–404). University of Arizona Press.

Nimmo, F., Pappalardo, R. T., & Giese, B. (2003). On the origins of band topography, Europa. *Icarus*, *166*, 21–32. https://doi.org/10.1016/j.icarus.2003.08.002

O'Brien, D. P., Geissler, P., & Greenberg, R. (2002). A melt-through model for chaos formation on Europa. *Icarus*, *156*(1), 152–161. https://doi.org/10.1006/icar.2001.6777

Paganini, L., Villanueva, G. L., Roth, L., Mandell, A. M., Hurford, T. A., Retherford, K. D., & Mumma, M. J. (2020). A measurement of water vapour amid a largely quiescent environment on Europa. *Nature Astronomy*, *4*(3), 266–272. (Number: 3 Publisher: Nature Publishing Group). https://doi.org/10.1038/s41550-019-0933-6

Pappalardo, R. T., Head, J. W., Greeley, R., Sullivan, R. J., Pilcher, C., Schubert, G., et al. (1998). Geological evidence for solid-state convection in Europa's ice shell. *Nature*, *391*, 365–368. https://doi.org/10.1038/34862

Patthoff, D. A., & Kattenhorn, S. A. (2011). A fracture history on Enceladus provides evidence for a global ocean. *Geophysical Research Letters*, *38*(18), L18201. https://doi.org/10.1029/2011GL048387

Petrenko, V. F., & Whitworth, R. W. (1999). *Physics of ice*. Oxford University Press.

Pleiner Sládková, K., Souček, O., & Běhounková, M. (2021). Enceladus' tiger stripes as frictional faults: Effect on stress and heat production. *Geophysical Research Letters*, *48*(19), e2021GL094849. https://doi.org/10.1029/2021GL094849

Porco, C. C., DiNino, D., & Nimmo, F. (2014). HOW the GEYSERS, tidal stresses, and thermal emission across the south polar terrain OF ENCELADUS are related. *The Astronomical Journal*, *148*(3), 45. https://doi.org/10.1088/0004-6256/148/3/45

Porco, C. C., Helfenstein, P., Thomas, P. C., Ingersoll, A. P., Wisdom, J., West, R., et al. (2006). Cassini observes the active south Pole of Enceladus. *Science*, *311*(5), 1393–1401. https://doi.org/10.1126/science.1123013

Postberg, F., Kempf, S., Schmidt, J., Brilliantov, N., Beinsen, A., Abel, B., et al. (2009). Sodium salts in E-ring ice grains from an ocean below the surface of Enceladus. *Nature*, *459*(7250), 1098–1101. https://doi.org/10.1038/nature08046

Quick, L. C., Glaze, L. S., & Baloga, S. M. (2017). Cryovolcanic emplacement of domes on Europa. *Icarus*, *284*, 477–488. https://doi.org/10.1016/j.icarus.2016.06.029

Roberts, J. H., & Stickle, A. M. (2021). Breaking the symmetry by breaking the ice shell: An impact origin for the south polar terrain of Enceladus. *Icarus*, *359*, 114302. https://doi.org/10.1016/j.icarus.2021.114302

Roth, L., Retherford, K. D., Saur, J., Strobel, D. F., Feldman, P. D., McGrath, M. A., & Nimmo, F. (2014). Orbital apocenter is not a sufficient condition for HST/STIS detection of Europa's water vapor aurora. *Proceedings of the National Academy of Sciences*, *111*(48), E5123–E5132. https://doi.org/10.1073/pnas.1416671111

Roth, L., Saur, J., Retherford, K. D., Strobel, D. F., Feldman, P. D., McGrath, M. A., & Nimmo, F. (2014). Transient water vapor at Europa's south Pole. *Science*, *343*(6167), 171–174. https://doi.org/10.1126/science.1247051

Rudolph, M. L., & Manga, M. (2009). Fracture penetration in planetary ice shells. *Icarus*, *199*(2), 536–541. https://doi.org/10.1016/j.icarus.2008.10.010

Schmidt, B. E., Blankenship, D. D., Patterson, G. W., & Schenk, P. M. (2011). Active formation of 'chaos terrain' over shallow subsurface water on Europa. *Nature*, *479*(7374), 502–505. https://doi.org/10.1038/nature10608

Schulson, E. M. (2001). Brittle failure of ice. *Engineering Fracture Mechanics*, *68*(17–18), 1839–1887. https://doi.org/10.1016/s0013-7944(01)00037-6

Shoji, D., Hussmann, H., Sohl, F., & Kurita, K. (2014). Non-steady state tidal heating of Enceladus. *Icarus*, *235*, 75–85. https://doi.org/10.1016/j.icarus.2014.03.006

Singer, K. N., McKinnon, W. B., & Schenk, P. M. (2021). Pits, uplifts and small chaos features on Europa: Morphologic and morphometric evidence for intrusive upwelling and lower limits to ice shell thickness. *Icarus*, *364*, 114465. https://doi.org/10.1016/j.icarus.2021.114465

Siraj, A., & Loeb, A. (2021). Repeated impact-driven plume formation on Enceladus over megayear timescales. *Icarus*, *357*, 114281. https://doi.org/10.1016/j.icarus.2020.114281

Sotin, C., Head, J. W., III, & Tobie, G. (2002). Europa- Tidal heating of upwelling thermal plumes and the origin of lenticulae and chaos melting. *Geophysical Research Letters*, *29*(8), 74–81. https://doi.org/10.1029/2001gl013844

Souček, O., Běhounková, M., Čadek, O., Hron, J., Tobie, G., & Choblet, G. (2019). Tidal dissipation in Enceladus' uneven, fractured ice shell. *Icarus*, *328*, 218–231. https://doi.org/10.1016/j.icarus.2019.02.012

Sparks, W. B., Hand, K. P., McGrath, M. A., Bergeron, E., Cracraft, M., & Deustua, S. E. (2016). Probing for evidence of plumes ON Europa with HST/STIS. *The Astrophysical Journal*. (Vol. *829*, 2. p. 121). American Astronomical Society. https://doi.org/10.3847/0004-637x/829/2/121

Sparks, W. B., Schmidt, B. E., McGrath, M. A., Hand, K. P., Spencer, J. R., Cracraft, M., & Deustua, S. E. (2017). Active cryovolcanism on Europa? *The Astrophysical Journal Letters*, *839*(2), L18. https://doi.org/10.3847/2041-8213/aa67f8

Steinbrügge, G., Voigt, J. R. C., Wolfenbarger, N. S., Hamilton, C. W., Soderlund, K. M., Young, D. A., et al. (2020). Brine migration and impact-induced cryovolcanism on Europa. *Geophysical Research Letters*, *47*(21), e2020GL090797. https://doi.org/10.1029/2020GL090797

Tobie, G., Čadek, O., & Sotin, C. (2008). Solid tidal friction above a liquid water reservoir as the origin of the south pole hotspot on Enceladus. *Icarus*, *196*(2), 642–652. https://doi.org/10.1016/j.icarus.2008.03.008

Turcotte, D. L., & Schubert, G. (2002). *Geodynamics* (2nd ed.). Cambridge University Press.

Ultee, L., Meyer, C., & Minchew, B. (2020). Tensile strength of glacial ice deduced from observations of the 2015 eastern Skaftá cauldron collapse, Vatnajökull ice cap, Iceland. *Journal of Glaciology*, *66*, 1–1033. https://doi.org/10.1017/jog.2020.65

Vilella, K., Choblet, G., Tsao, W.-E., & Deschamps, F. (2020). Tidally heated convection and the occurrence of melting in icy satellites: Application to Europa. *Journal of Geophysical Research: Planets*, *125*(3), e2019JE006248. https://doi.org/10.1029/2019JE006248

Walker, C. C., Bassis, J. N., & Schmidt, B. E. (2021). Propagation of vertical fractures through planetary ice shells: The role of basal fractures at the ice-ocean interface and proximal cracks. *The Planetary Science Journal* (Vol. *2*, 4 p. 135). PublisherIOP Publishing. https://doi.org/10.3847/PSJ/ac01ee

Weeks, W. F. (1962). Tensile strength of NaCl ice. *Journal of Glaciology*, *4*(31), 25–52. https://doi.org/10.3189/S0022143000018190

Wilson, L., Head, J. W., & Pappalardo, R. T. (1997). Eruption of lava flows on Europa: Theory and application to Thrace Macula. *Journal of Geophysical Research: Planets*, *102*(E4), 9263–9272. https://doi.org/10.1029/97je00412